Sensors and Materials, Vol. 36, No. # (2024) 1–9
MYU Tokyo

S & M ####

Calculation of Photocatalyst Anatase TiO_2 (1 0 1)/g-C_3N_4 (0 0 1) Properties Using Density Functional Theory

Trung Tin Tran,[1,2,4] Phuoc Thao Vo Du,[2,4]
Anh Hao Huynh Vo,[3,4] and Trung Nghia Tran[3,4*]

[1]Faculty of Physics and Physics Engineering, University of Science, VNUHCM, Ho Chi Minh City, Vietnam
[2]Department of Engineering Physics, Faculty of Applied Science, Ho Chi Minh City University of Technology, 268 Ly Thuong Kiet Street, District 10, Ho Chi Minh City, 72409 Vietnam
[3]Laboratory of Laser Technology, Faculty of Applied Science, Ho Chi Minh City University of Technology, 268 Ly Thuong Kiet Street, District 10, Ho Chi Minh City, 72409 Vietnam
[4]Vietnam National University Ho Chi Minh City, Linh Trung Ward, Thu Duc City, Ho Chi Minh City, 71308 Vietnam

(Received August 21, 2023; accepted November 29, 2023)

Keywords: anatase TiO_2, g-C_3N_4, heterostructure, visible-light photocatalyst, density functional theory

Titanium dioxide (TiO_2), a metal oxide photocatalyst, is one of the most widely studied materials for photocatalytic applications in energy production and environmental remediation owing to its excellent photocatalytic performance. Recently, graphitic carbon nitride (g-C_3N_4) has gained a widespread photocatalytic application owing to its band gap of 2.70 eV, good physicochemical stability, ease of processing, and low cost. However, the photocatalytic performance characteristics of TiO_2 and g-C_3N_4 determined individually have been confirmed by researchers to be unsatisfactory for heterogeneous photocatalysis owing to the high recombination capacity of photogenerated electron–hole pairs and the low energy conversion efficiency. A theoretical understanding of the relationship between the interfaces of TiO_2 and g-C_3N_4 is still lacking. In this study, we investigated the effects of the interface structure on the electronic properties of the anatase TiO_2/g-C_3N_4 heterostructure using density functional theory (DFT) calculations. The interaction between the anatase TiO_2 surface and the g-C_3N_4 monolayer with (1 0 1)/(0 0 1) facets has been revealed, where a van der Waals heterojunction is formed. The anatase TiO_2 (1 0 1)/g-C_3N_4 (0 0 1) heterostructure has a narrow band gap (1.876 eV) shown by DFT calculation. It effectively separates electron–hole pairs, leading to a strong optical absorption ability in the visible light region with a maximum absorption wavelength of 661 nm. The strengthened separation of electron–hole pairs and the restrained carrier recombination in the g-C_3N_4/TiO_2 interface were analyzed on the basis of the Z-scheme photocatalytic mechanism. The results suggest that the anatase TiO_2 (1 0 1)/g-C_3N_4 (0 0 1) heterostructure is a promising material for photocatalytic applications.

*Corresponding author: e-mail: ttnghia@hcmut.edu.vn

ISSN 0914-4935

1. Introduction

Photocatalysis is present in a wide range of applications including energy storage and conversion, and environmental remediation. Titanium dioxide (TiO_2) is one of the well-known semiconductor photocatalysts despite its low efficiency owing to its wide band gap. This limitation leads to the underutilization of the vast excitation source from solar energy.[1] Therefore, researchers want to develop new photocatalysts based on TiO_2 with high catalytic activity. In addition, these new photocatalysts have good photogenerated charge separation in a wide response wavelength range. Recently, their photocatalytic performance improvement has been based on the controlled growth of the characteristic crystal facets of semiconductors. The facets of anatase TiO_2 were found to be beneficial for the transfer of photogenerated carriers, thus enhancing its photocatalytic activity.[2–7]

Graphitic carbon nitride (g-C_3N_4), which is an n-type layered semiconductor, has a special structure and electronic properties that make it an effective photocatalyst for hydrogen production under visible light.[8–10] However, the limitation of g-C_3N_4 is in the high recombination rate of photogenerated electron–hole pairs as well as the high band gap energy.[11, 12]

The coupling of TiO_2 with g-C_3N_4 into a new composite material structure has been explored to improve photocatalytic activity and photogenerated charge separation. This was considered an effective method to overcome the limitations of these two separate materials by the fast electron transfer at the interface of the formed heterojunction.[13,14] The g-C_3N_4/TiO_2 heterostructures were also used as novel materials for photo-electrochemical biosensors.[15, 16] In this way, there is an improvement in the poorly visible light excitation of TiO_2 and the retardation of charge recombination on g-C_3N_4, which contributes to the improved performance of the photo-electrochemical sensor. This improves the efficiency by 350% compared with those of other sensors. The performance of a photo-electrochemical glucose enzymatic biosensor was improved with a linear range of 0.05–16 mM and a line detection limit of 0.01 mM.[17]

The interaction between the g-C_3N_4 interface and different sides of TiO_2 has not been fully revealed, which limits our understanding of how combining these two materials affects their properties. Moreover, the enhancement of the photoactivity and the inhibition of the electron–hole pair recombination of the TiO_2/g-C_3N_4 heterostructure are still in the research and clarification stages. Density functional theory (DFT) has emerged as a powerful computational method in the field of materials science. DFT offers a quantum mechanical framework to study the electronic structure and properties of various systems. Using DFT, Oprea and Gîrțu studied the electronic structure and properties of TiO_2 nanoclusters for hybrid photovoltaic and photocatalysis reactions.[18] Li *et al.* used DFT calculations to demonstrate the increasing band gap of cotton fibers modified with g-C_3N_4/TiO_2 after synthesis by a hydrothermal method.[19]

In this study, we used the DFT method to help us determine the effects of the electronic properties of photocatalysts, the interaction between the different components in a combined structure, and the chemical reaction process on the interface of the anatase TiO_2 (1 0 1)/g-C_3N_4 (0 0 1) heterostructure.

2. Modeling and Computational Method

In this study, we built a model of the TiO_2/g-C_3N_4 heterostructure formed by surface TiO_2 (1 0 1) and g-C_3N_4 (0 0 1). The DFT method is used to calculate the electronic structure of the materials and the interaction between these materials' models, thereby predicting and explaining the mechanism that increases the photocatalytic activity of materials for proving the role of the TiO_2/g-C_3N_4 material with high efficiency in the visible light region. BIOVIA Materials Studio is the tool used to model the structure and calculate the characteristic properties of materials with CASTEP and DFTB+ modules.

2.1 Modeling anatase TiO_2 (1 0 1)/g-C_3N_4 (0 0 1) structure

The TiO_2/g-C_3N_4 model was built by placing the monolayer model of g-C_3N_4 (0 0 1) on the surface of the anatase TiO_2 (1 0 1) model. This process consists of two main steps: (1) building the unit cell of these materials and (2) perfecting the structural geometry. Figure 1 shows the models built in this study, including the structures of monolayer g-C_3N_4 [Fig. 1(a)] and anatase TiO_2 [Fig. 1(b)] with their unit sizes of 1 × 1 × 1 and 2 × 2 × 2, respectively. The anatase TiO_2 crystal has a tetragonal structure, and its space group is I 41/a m d, whereas the g-C_3N_4 layer has

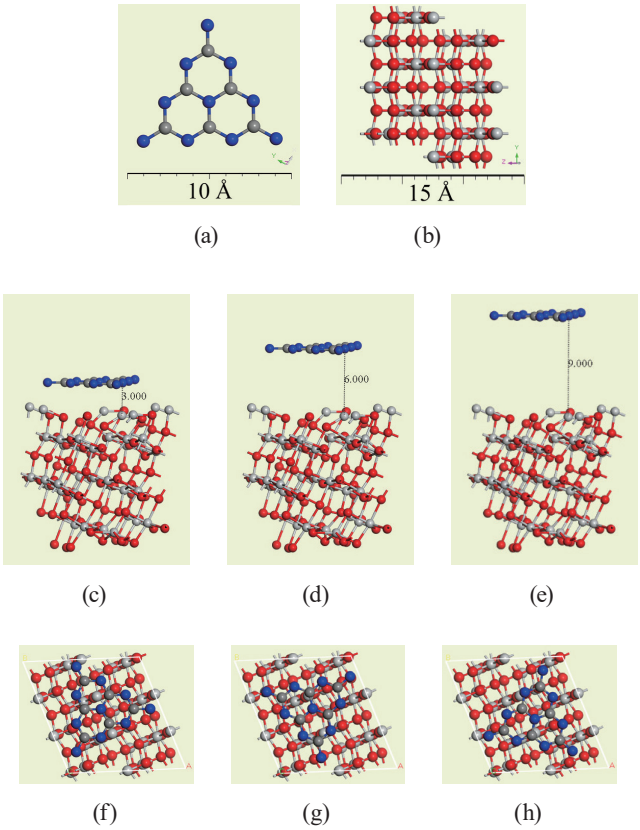

Fig. 1. (Color online) (a) Monolayer g-C_3N_4 (0 0 1), (b) anatase TiO_2 (1 0 1), and initial TiO_2/g-C_3N_4 models with (c)–(e) different distances and (f)–(h) placement angles.

a hexagonal P-6m2 space group. The built pseudo-cyclic network of the TiO_2/g-C_3N_4 tetragonal structure has the lattice constants $a = b = 10$ Å and $c = 20$ Å and the angles $\alpha = \beta = 90°$ and $\gamma = 120^o$. When these materials are combined, the g-C_3N_4 monolayer can bind to the TiO_2 surface in distinct positions. Therefore, we also investigated the effects of the various initial positions of these two layers on the optimized model's result. The different investigated locations were associated with different distances of 3, 6, and 9 Å [Figs. 1(c)–1(e)] and different random initial angles [Figs. 1(f)–1(h)] of the g-C_3N_4 layer on the TiO_2 model.

2.2 Computational methods

The anatase TiO_2 model and g-C_3N_4 monolayer were optimized to obtain properties consistent with experimental studies, then the calculation process based on the combination of these two optimized models was performed using DFTB+. For describing the exchange and correlation potentials of the built models, the generalized gradient approximations based on the Perdew–Burke–Ernzerhof functional (GGA-PBE) were used. The models were optimized under a plane-wave cutoff energy of 500 eV with the Monkhorst–Pack k-point grids of 5 × 5 × 2 for the TiO_2 structure and 2 × 2 × 2 for the g-C_3N_4 monolayer. The Heyd–Scuseria–Ernzerhof (HSE06) hybrid functional was used to construct the anatase TiO_2 and g-C_3N_4 models similar to previous reports,[20–23] with energy band gap values of approximately 3.2 and 2.7 eV, respectively. The configurations of electrification considered in this study include Ti ($4s^2$ $3d^2$), O ($2s^2$ $2p^4$), N ($2s^2$ $2p^3$), and C ($2s^2$ $2p^2$). Because the DFT method ignores the interaction between valence electrons of the atoms in the solid, the Hubbard U parameter of 8.2 eV was also applied to the 3d orbital of the Ti element.

3. Results

3.1 Anatase TiO_2 and g-C_3N_4 models

The optimized structures' results of the anatase TiO_2 crystal and g-C_3N_4 monolayer models are shown in Table 1. After the optimization, the lattice constants of the anatase TiO_2 crystal model are $a = b = 3.79$ Å and $c = 9.67$ Å and the angles are $\alpha = \beta = \gamma = 90°$. When comparing these results with the JCPDS Card no. 21-1272 (anatase TiO_2), the difference is only about 0.515%. For the g-C_3N_4 monolayer model, the lattice constants are $a = b = 7.11$ Å and $c = 6.5$ Å and the angles are $\alpha = \beta = 90^o$ and $\gamma = 120^o$.

Figure 2 shows the electronic structure calculation results after optimizing the geometric structure of the built models, in which the horizontal dashed line is the Fermi level of the material corresponding to the zero-energy level. The band gap energy values of anatase TiO_2

Table 1
Calculated lattice constants of anatase TiO_2 crystal and g-C_3N_4 monolayer models.

Lattice constants	a (Å)	b (Å)	c (Å)	α (deg)	β (deg)	γ (deg)
Anatase TiO_2	3.79	3.79	9.67	90°	90°	90°
g-C_3N_4	7.11	7.11	6.5	90°	90°	120°

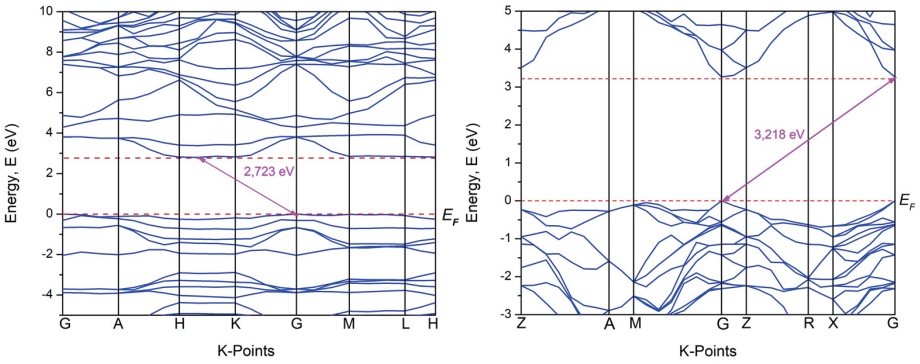

Fig. 2. (Color online) Energy band structures of (a) anatase TiO_2 crystal and (b) g-C_3N_4 monolayer models.

and g-C_3N_4 from their energy band structures are 3.218 and 2.723 eV, respectively. These results are consistent with previously reported studies on these two materials.[20–23] The obtained results of the spatial structures (as shown in Table 1) as well as the energy band structures (as shown in Fig. 2) revealed that the two separate simulations of the built models are suitable for investigating the heterostructure when combining anatase TiO_2 and g-C_3N_4.

3.2 Anatase TiO_2 (1 0 1)/g-C_3N_4 (0 0 1) heterostructure

The optimization results of the geometric structure of TiO_2/g-C_3N_4 are shown in Fig. 3(a). The shortest distances between the C atom and the anatase TiO_2 (1 0 1) facet are about 2.467 and 3.569 Å, which correspond to the distances from the C atom to the O and Ti atoms [Fig. 3(b)], respectively. At the same time, these minimum distances from the N atom to the Ti and O atoms in the order given [Fig. 3(c)] are 2.603 and 2.153 Å, respectively. The interaction between the g-C_3N_4 (0 0 1) monolayer and the anatase TiO_2 (1 0 1) surface is weak because van der Waals heterojunctions are formed.

Compared with that of the pure anatase TiO_2 model, the band gap of the anatase TiO_2 (1 0 1)/g-C_3N_4 (0 0 1) heterostructure (as shown in Fig. 4) is reduced to 1.876 eV by the interaction between the anatase TiO_2 (1 0 1) surface and the g-C_3N_4 (0 0 1) monolayer. This result means that electrons are easier to excite from the valence band (VB) to the conduction band (CB) in the anatase TiO_2/g-C_3N_4 heterostructure. There is a shift of the optical absorption boundary, in which the maximum absorption wavelength is determined using the equation

$$\lambda_{max} = \frac{hc}{E_g} = \frac{\left(6.62607015\times10^{-34}\right)\times\left(299792458\right)}{1.876\ \times\left(1.602177\times10^{-19}\right)}\times10^{9} \approx 661\ \text{nm},$$

where h is Planck's constant, c is the speed of light, and E_g is the band gap of the anatase TiO_2 (1 0 1) / g-C_3N_4 (0 0 1) heterostructure. The calculation shows that the material absorbs light well in the visible light region of about 661 nm.

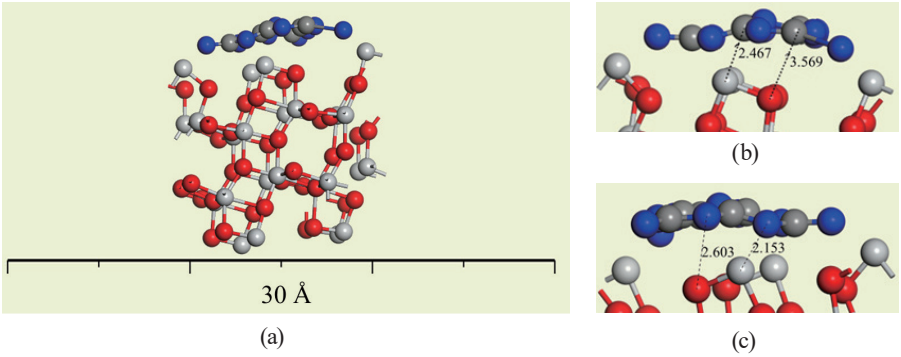

Fig. 3. (Color online) (a) Anatase TiO_2 (1 0 1)/g-C_3N_4 (0 0 1) after structure optimization process, (b) closest distance between carbon atom and anatase TiO_2 (1 0 1) facet, and (c) closest distance between nitrogen atom and anatase TiO_2 (1 0 1) facet.

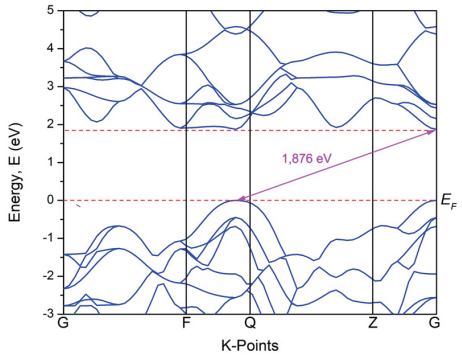

Fig. 4. (Color online) Energy band structure of anatase TiO_2 (1 0 1)/g-C_3N_4 (0 0 1) heterostructure.

The total state density of anatase TiO_2 (1 0 1)/g-C_3N_4 (0 0 1) [Fig. 5(a)] shows that the VB and CB of TiO_2/g-C_3N_4 are in the energy range from −12.0 to +10.0 eV. The energy levels include those in the CB located in the upper part of the chart and those in the VB located in the rest. In the heterostructure of anatase TiO_2 (1 0 1)/g-C_3N_4 (0 0 1), the valence band maximum (VBM) is structured by the N 2p state closer to the O 2p state, whereas the conduction band minimum (CBM) is composed of 3d Ti states [as shown in Fig. 5(b)]. The VBM and CBM of the g-C_3N_4 layer are higher than those of the anatase TiO_2 (1 0 1) facet bands, which indicates the possible existence of staggering band bonding in the heterostructured anatase TiO_2 (1 0 1)/g-C_3N_4 (0 0 1).

For pure anatase TiO_2, most photo-excited electron and hole carriers tend to recombine before they reach their destination to participate in the catalytic reaction. Therefore, the photocatalytic activity is not good under the excitation's visible spectrum. However, for the anatase TiO_2/g-C_3N_4 heterostructure, the surface leads to the formation of a Z-scheme system between anatase TiO_2 and g-C_3N_4. Under visible light irradiation, the photo-induced holes tend to stay on the VB of anatase TiO_2, whereas the electrons transfer to the VB of g-C_3N_4 from the CB of anatase TiO_2. The electrons in the g-C_3N_4 layer's VB are further excited to its CB. This

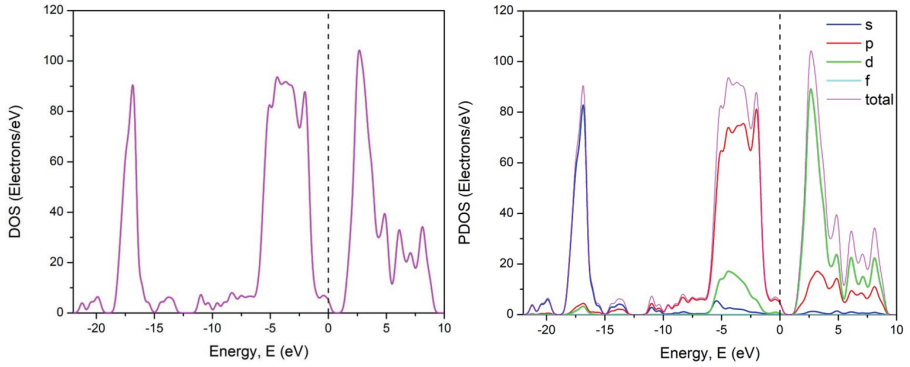

(a) (b)

Fig. 5. (Color online) (a) Total and (b) partial densities of states of anatase TiO_2 (1 0 1)/g-C_3N_4 (0 0 1).

process leads to the effective spatial separation of charge carriers caused by photovoltaics. Then, the electrons stored in the CB of g-C_3N_4 will participate in the reaction processes. This is especially beneficial when it is possible to take advantage of the excitation from solar energy. The calculation results of the anatase model TiO_2 (1 0 1)/g-C_3N_4 (0 0 1) are also confirmed when the band gap energy of this heterostructure model is only 1.867 eV, which corresponds to the absorbance wavelength photon peak in the visible region (661 nm). At the same time, this energy is also significantly smaller than that calculated from the individual anatase TiO_2 and g-C_3N_4 models (3.218 and 2.723 eV, respectively). Therefore, the photocatalytic activity of anatase TiO_2 (1 0 1)/g-C_3N_4 (0 0 1) under visible light is enhanced owing to the better utilization of the excitation source based on the Z-scheme charge transfer model.

4. Conclusions

We performed DFT calculations on the anatase TiO_2 (1 0 1)/g-C_3N_4 (0 0 1) heterostructure to explain the mechanism of increasing the material's photocatalytic activity. To build this model structure, the anatase TiO_2 (1 0 1) facet was considered to combine with the g-C_3N_4 (0 0 1) surface. The interaction between g-C_3N_4 and the anatase TiO_2 surface is weak and formed by van der Waals heterojunctions. The anatase TiO_2 (1 0 1)/g-C_3N_4 (0 0 1) heterostructure has a band gap of 1.876 eV, which is narrower than those of component materials. This calculated result is due to the staggering linkage in the anatase TiO_2 (1 0 1)/g-C_3N_4 (0 0 1) heterostructure, which is based on the Z-scheme mechanism. When combining the two materials, anatase TiO_2 and g-C_3N_4, the densities of states forming the VB and CB change. The VBM of the heterostructure model is structured by the N 2p state, whereas its CBM is composed of 3d Ti states. The band gap energy, which is calculated from the anatase TiO_2 (1 0 1)/g-C_3N_4 (0 0 1) model, contributes to explaining the light absorption capacity of this structure in the visible region.

Acknowledgments

This research was funded by Vietnam National University Ho Chi Minh City (VNU-HCM) under grant number B2022-20-01/HĐ-KHCN. We acknowledge the Ho Chi Minh City University of Technology (HCMUT), VNU-HCM for supporting this study.

Conflicts of Interest

The authors declare no conflict of interest.

References

1 D. R. Eddy, M. D. Permana, L. K. Sakti, and G. A. N. Sheha: Nanomaterials **13** (2023) 704. https://doi.org/10.3390/nano13040704
2 Y. Gui, W. Li, X. He, Z. Ding, C. Tang, and L. Xu: Appl. Surf. Sci. **507** (2020) 145163. https://doi.org/10.1016/j.apsusc.2019.145163
3 L. Jiang and G. Zhou: Appl. Surf. Sci. **535** (2021) 147709. https://doi.org/10.1016/j.apsusc.2020.147709
4 X. Li, Z. Shen, H. Zhang, X. Li, Y. Zhou, and H. Yao: Chem. Eng. J. **440** (2022) 135665. https://doi.org/10.1016/j.cej.2022.135665
5 J. Li, C. Zhang, Q. Li, T. Gao, S. Yu, P. Tan, Q. Fang, and G. Chen: Chem. Eng. Sci. **251** (2022) 117438. https://doi.org/10.1016/j.ces.2022.117438
6 H. Wu, J. Bian, Z. Zhang, Z. Zhao, S. Xu, Z. Li, N. Jiang, E. Kozlova, X. Hua, and L. Jing: Appl. Surf. Sci. **623** (2023) 157066. https://doi.org/10.1016/j.apsusc.2023.157066
7 R. Katal, S. Masudy-Panah, M. Tanhaei, M. H. D. A. Farahani, and H. Jiangyong: Chem. Eng. J. **384** (2020) 123384. https://doi.org/10.1016/j.cej.2019.123384
8 C. Prasad, H. Tang, Q. Liu, I. Bahadur, S. Karlapudi, and Y. Jiang: Int. J. Hydrogen Energy **45** (2020) 337. https://doi.org/10.1016/j.ijhydene.2019.07.070
9 S. R. Nagella, R. Vijitha, B. Ramesh Naidu, K. S. V. Krishna Rao, C.-S. Ha, and K. Venkateswarlu: Nano Energy **111** (2023) 108402. https://doi.org/10.1016/j.nanoen.2023.108402
10 Q. Xu, D. Ma, S. Yang, Z. Tian, B. Cheng, and J. Fan: Appl. Surf. Sci. **495** (2019) 143555. https://doi.org/10.1016/j.apsusc.2019.143555
11 C. Feng, X. Ouyang, Y. Deng, J. Wang, and L. Tang: J. Hazard. Mater. **441** (2023) 129845. https://doi.org/10.1016/j.jhazmat.2022.129845
12 Z. Shi, L. Rao, P. Wang, and L. Zhang: Environ. Sci. Pollut. Res. **29** (2022) 83981. https://doi.org/10.1007/s11356-022-21535-w
13 R. Acharya, and K. Parida: J. Environ. Chem. Eng. **8** (2022) 103896. https://doi.org/10.1016/j.jece.2020.103896
14 P. John, K. Johari, N. Gnanasundaram, A. Appusamy, and M. Thanabalan: Environ. Technol. Innovation **22** (2021) 101412. https://doi.org/10.1016/j.eti.2021.101412
15 Y. Wang, X. Li, G. I. N. Waterhouse, Y. Zhou, H. Yin, and S. Ai: Talanta **196** (2019) 197. https://doi.org/10.1016/j.talanta.2018.12.035
16 S. S. Low, Z. Chen, Y. Li, Y. Lu, and Q. Liu: TrAC, Trends Anal. Chem. **145** (2021) 116454. https://doi.org/10.1016/j.trac.2021.116454
17 P. Liu, X. Huo, Y. Tang, J. Xu, X. Liu, and D. K. Y. Wong: Anal. Chim. Acta **984** (2017) 86. https://doi.org/10.1016/j.aca.2017.06.043
18 C. I. Oprea and M. A. Gîrțu: Nanomaterials **9** (2019) 375. https://doi.org/10.3390/nano9030357
19 W. Li, H. Zhang, W. Chen, L. Yang, H. Wu, and N. Mao: Cellulose **29** (2022) 193. https://doi.org/10.1007/s10570-021-04318-3
20 R. B. Rajput, S. N. Jamble, and R. B. Kale: Engineered Science **17** (2022) 176. https://doi.org/10.30919/es8d534
21 A. Sharma, P. Negi, R. J. Konwar, H. Kumar, Y. Verma, Shailja, P. C. Sati, B. Rajyaguru, H. Dadhich, N. A. Shah, and P. S. Solanki: J. Mater. Sci. Technol. **111** (2022) 287. https://doi.org/10.1016/j.jmst.2021.09.014
22 A. Hayat, A. G. Al-Sehemi, K. S. El-Nasser, T. A. Taha, A. A. Al-Ghamdi, J. A. S. Syed, M. A. Amin, T. Ali, T. Bashir, A. Palamanit, J. Khan, and W. I. Nawawi: Int. J. Hydrogen Energy **47** (2022) 5142. https://doi.org/10.1016/j.ijhydene.2021.11.133
23 S. Sahoo and R. Acharya: Mater. Today Proc. **35** (2021) 150. https://doi.org/10.1016/j.matpr.2020.04.008

About the Authors

Trung Tin Tran received his B.S. and M.S. degrees from the University of Science (HCMUS), VNUHCM, Vietnam, in 2014 and 2019, respectively. Since 2016, he has been a reseacher at Ho Chi Minh City University of Technology (HCMUT), VNUHCM, Vietnam. His research interests are in nanomaterials, bioengineering, and sensors. (trtrtin@hcmut.edu.vn)

Phuoc Thao Vo Du received his B.E. degree from Ho Chi Minh City University of Technology (HCMUT), VNUHCM, Vietnam, in 2022. (thao.vo2000@hcmut.edu.vn)

Anh Hao Huynh Vo received his B.E. degree from Ho Chi Minh City University of Technology (HCMUT), VNUHCM, Vietnam, in 2021. Since 2021, he has been a graduate student at HCMUT, VNUHCM. Since 2023, he has also been a research assistant at HCMUT, VNUHCM. (hvahao@hcmut.edu.vn)

Trung Nghia Tran received his B.E. and M.S. degrees from Ho Chi Minh City University of Technology (HCMUT), VNUHCM, Vietnam, in 2005 and 2010, respectively, and his D. Eng. degree from Hokkaido University, Japan, in 2014. Since 2006, he has been a lecturer at Ho Chi Minh City University of Technology (HCMUT), VNUHCM, Vietnam. His research interests are in biomedical optics, bioimpedance, electrical impedance tomography, and photobiomodulation. (ttnghia@hcmut.edu.vn)